IEEE Access
Multidisciplinary ⋮ Rapid Review ⋮ Open Access Journal

Received 17 September 2022, accepted 14 October 2022, date of publication 19 October 2022, date of current version 26 October 2022.

Digital Object Identifier 10.1109/ACCESS.2022.3215957

RESEARCH ARTICLE

Multi-Class Prediction of Mineral Resources Based on Deep Learning

LIANG DING[1], YUELONG ZHU[1], PENGCHENG ZHANG[1], (Member, IEEE), HAI DONG[2], (Senior Member, IEEE), AND HAO CHEN[1]

[1]College of Computer and Information, Hohai University, Nanjing 211100, China
[2]School of Computing Technologies, RMIT University, Melbourne, VIC 3000, Australia

Corresponding author: Liang Ding (dingliang2017@hhu.edu.cn)

This work was supported by the Natural Science Foundation of China under Grant 61572171.

ABSTRACT Big data-driven technologies, especially machine learning and deep learning technologies, have been extensively employed in mineral prospectivity prediction. Several approaches have been proposed to learn the deep characteristics of geoscience data, enhance the accuracy of prediction and reduce uncertainty. Nevertheless, the approaches always contain the following two limitations. Firstly, the formation of mineral resources often involves the coupling of multiple factors on a certain spatio-temporal scale, resulting in rare labelled deposits and insufficient number of training samples. Secondly, training Deep Neural Network (DNN) is very challenging. Many approaches are subject to weak interpretability and lack of organic combination with geoscience knowledge. To address these two problems, we propose Geo-Rnet and GCAE (Geological Convolutional Autoencoder). Geo-Rnet is a multi-class mineral prospectivity prediction approach based on improved DNN. GCAE is able to effectively augment multi-disciplinary geoscience data by constructing upon an optimized Convolutional Autoencoder. The experimental results show that most of prospective areas predicted by Geo-Rnet overlap with the labelled mineralization locations, with an average accuracy of 91.1%. In addition, 89.98% of the ore deposits are located in the predicted areas. The results indicate the effectiveness of Geo-Rnet and GCAE for multi-class prediction of mineral resources. Finally, we classify the target area into several mineral prospectiviy areas according to their different mineral types. The research provides an innovative approach for mineral prospectivity prediction in the target area.

INDEX TERMS Deep neural network, Geo-Rnet, multi-class, mineral prediction.

I. INTRODUCTION

Mining of geoscience data is at the frontier of mineral resources prediction research [1]. Previously mineral resources prediction was based on similar analogy approaches, mainly qualitative prediction and knowledge driven methods to discover similar metallogenic environment of deposits [2]. Along with the development of geoscience, such as the use of quantitative models in Geographic Information System (GIS) for mineral resources prediction, expert knowledge is expressed in a more structured and logical way. Some researchers employed both data and knowledge to drive predictive research [3], [4], [5]. The common approach is to build a physical model for the formation of the deposit, and analyze the deposit formation source, transport, storage and so on. Based on physical model, researchers employ a variety of approaches to extract and identify the characteristics of geoscience spatial variables, and finally fuse and delineate the mineral prospectivity mapping (MPM) [6], [7], [8], [9]. With the enhancement of approaches for geoscience survey data acquisition, geoscience data gradually show the characteristics of high volume and diversity in types, sources, scales and so on [5].

In recent years, with the explosive growth of computational capabilities and data volume, machine learning and artificial intelligence have achieved rapid development, and demonstrated a strong analytical and predictive ability in geoscience big data research [10], [11]. [12], [13], [14], [15], [16], [17], [18], [19], [20], [21], [22] employed various supervised learning methods in machine learning, by which

The associate editor coordinating the review of this manuscript and approving it for publication was Mohamed Elhoseny.

the data features of the spatial locations of known mineral resources were mined. These approaches achieved promising prediction effect in target areas. [23], [24], [25] employed various unsupervised learning methods in machine learning (ML), by reconstructing the geochemical data to extract the anomaly and mining the spatial locations of the anomaly data, to carry out the prediction research. In addition, [26] employed the method combining supervised learning and unsupervised learning to conduct a prediction research on mineral resources.

Although these aforementioned approaches have made distinct progress in the multi-class prediction of mineral resources, mineral prediction still suffers from the following two main challenges:

1) Insufficient labelled mineral resources samples. The geoscience data are scattered and heterogeneous, and the metallogenic activity is localized, and the formation of mineral resources is rare. The formation of mineral resources often involves the coupling of multiple factors on a certain spatio-temporal scale, resulting in rare labelled deposits and insufficient number of training samples [27].
2) Non-robustness of deep learning (DL) models. DNN is commonly treated as a black box, which subjects to weak interpretability and lack of organic combination with geoscience knowledge. The selection of different network structures, the depth of the same network, the scale of convolution, and the adjustment of loss function usually pose a great impact on the prediction results. A model may sometimes encounter problems such as unsatisfactory prediction results due to deeper network stacking effect and weak sensitivity to misclassification [3].

Many scholars have carried out exploratory studies in this field. For example, [28] proposed geological prospecting data augmentation techniques based on replication and noise addition as well as built convolutional neural network (CNN) models for geoscience data mining and integration. [26] aimed at the deep learning problems with few samples. The training data were constructed based on unsupervised learning approach, so that DNN can be effectively applied to mineral prediction. However, the traditional computer image data augmentation techniques may change the spatial features of geoscience data. Therefore, it is crucial to choose a compatible data augmentation approach that conforms to the feature of geoscience data.

On the basis of establishing the geoscience dataset in the target area, this paper proposes a multi-class prediction approach for mineral resources based on deep learning. In summary, the major contributions of this paper include the following three aspects:

1) We design Geo-Rnet, an innovative prediction model for handling the mineral resources multi-class problem. By optimizing the design of DNN architecture and hyperparameters, the model can avoid the problem of gradient dispersion caused by the excessive number of network layers, and enhance the robustness and transfer learning ability of the model. In addition, by optimizing the loss function, different mathematical calculation approaches are adopted for different types of samples, different weights or classification thresholds are adjusted to meet the multi-class requirements of unbalanced mineral resources data. The sensitivity of the model to misclassification is enhanced by improving the constraint of geoscience knowledge on the model.
2) We design GCAE, an optimized convolutional autoencoder network for data augmentation. We use GCAE to extract the depth features of the original geoscience data and augment the data according to these features. GCAE can identify abnormal data with geoscience features and serve as samples to enhance the training data and reduce the generalization error. It can also change the data distribution of the training data to eliminate or weaken the unbalanced state of small samples. We use GCAE to alleviate the data uninterpretability caused by traditional data augmentation approaches.
3) We design a series of experiments to evaluate the approach. The experiment verifies the effectiveness of the approach on improving the transferability of mineral resources samples after data reconstruction, and proves that Geo-Rnet and GCAE can improve the prediction accuracy of the model for potential mineral deposits in the target area.

The remainder of this paper is organized as follows: in Section 2 we introduce the geological background of the target area and the main influencing factors. In Section 3, we describe the proposed approaches. In Section 4, we discuss the experiment over multiple geoscience data.

II. TARGET AREA AND RELEVANT DATA

Mineral resources prediction is faced with a large number of geoscience data, such as geology, geophysics, geochemistry and so on, which are often characterized by multi-heterogeneity, multi-disciplinary and non-stationarity. The data in this research were generated by a geological survey project conducted in the middle and lower reaches of the Yangtze River [29]. The data include geological data, geochemical data, geophysical data and other data, at a scale of 1:200,000.

We use ArcGIS software[1] to transform the coordinates of these data, unify the geographic and projection coordinate systems, and establish the spatial and attribute data of the target area. After data processing, reconstruction and analysis, we extract the spatial and geological attributes of the known multi-type copper ore deposits and related elements of the target area.

A. TARGET AREA

The target area is in Nanjing, Jiangsu, China. It is located in the Lower Yangtze River belts. The target area is about

[1] https://www.esri.com/

1 square kilometers, which contains main minerals including iron, copper, lead, zinc, strontium, pyrite and other 58 species.[2] The area is the main distribution area of large and medium-sized copper, iron and gold ore deposits along the middle and lower reaches of the Yangtze River metallogenic belt, which is called the main body of the Yangtze River metallogenic belt. There are many types of ore deposits and dense distribution of mineral producing areas. In addition to the absence of the Middle and lower Devonian and part of the Lower Carboniferous, there are outcrops from the Precambrian to the Quaternary, in which Carboniferous, Permian and Middle and Lower Triassic carbonate rocks and Upper Jurassic to Lower Cretaceous continental volcanic rocks are the main ore-forming and ore-hosting rocks. All the deposits are controlled by the tracing Yangtze River deep fault. Although the magmatic series are different in formation age and metallogenic features, their mineralization is unified in the tectono-magmatic thermal events developed mainly in the Mesozoic Yanshanian period, forming the main tectono-magmatic metallogenic subbelt with characteristics in the middle and lower reaches of the Yangtze River [3], [29], [30].

B. RELEVANT DATA

In this section, we introduce the data related to the prediction of mineral resources in the target area. All the geoscience data are transformed into unified spatial data through ArcGIS, in which rocks, faults, geophysical data are respectively fed as a channel and all the (39) elements of geochemical exploration data form the data of 39 channels. Finally, the experimental data are spatial raster data with 42 data channels. For experimental comparison, 10 major chemical elements are selected based on [29] and combined with geological and other data to form spatial raster data with 13 channels.

1) INTRUSIVE ROCKS AND VOLCANIC ROCKS

The Yanshanian magmatic activity was strong in the target area. Large-scale and multi-period magmatic intrusion and volcanic eruption occurred in the Early Cretaceous. There are various types of magmatic rocks formed in the area, including intermediate basic-medium acidic and alkaline lithology, mainly volcanic rocks, and secondary intrusive rocks, with a wide distribution range. The contact zone of Carbonate rocks and intrusive rocks is a favorable area for mineralization in the northern part of the area. In the southern part of the region, the formation of different mineral deposits and different types of deposits is related to volcanic-intrusive activities of each subcycle in the late Yanshanshan period. Intrusive rocks and volcanic rocks are the main sources of mineral resources in this area. In this research, spatial data of rock mass are generated by establishing Euclidean distance.

2) FAULTS

In the northern part of the target area, the NE (North East)-trending and NW (North West)-trending Yangtze River deep fault zone meshes control the stratigraphic distribution and the distribution of ore deposits. In the southern part of the district, it is mainly controlled by fault grid and volcanic mechanism formed by NNE (North North East)-trending, NEE (North East East)-trending, NW-trending and other faults criss-cross in the district. The faults in this area are the main channels for the formation of mineral resources, and the intersection points of faults are prone to mineralization. In this paper, the spatial data of faults are generated by establishing the density of fault intersections.

3) GEOPHYSICAL

In the northern part of the target area, the aeromagnetic anomaly shows a wide abnormity zone with positive and negative association. The negative magnetic field in the north is wide and slow, and the positive magnetic field gradient in the south is large. In the southern part of the district, the spatial distribution of local anomalies is mostly northeast-oriented ribbon with different amplitude. In this paper, geophysical data are extracted as model input by interpolation.

4) GEOCHEMICAL

The geochemical data in the target area include 39 elements, such as *Ag*, *As*, *Au*, *Ba*, *Be*, *Bi*, *Cd*, *Co*, *Cr*, *Cu*, *F*, *Hg*, *La*, *Li*, *Mn*, *Mo*, *Nb*, *Ni*, *Pb*, *Sb*, *Sn*, *Sr*, *Th*, *Zn*, *Zr*, etc. All the original data are converted into spatial data by the IDW (Inverse Distance Weighted) tool in ArcGIS software. In addition, 10 major elements (*Ag*, *As*, *Au*, *Hg*, *Mn*, *Mo*, *Pb*, *Sb*, *Sn*, *Zn*) [29] are selected as the training data of the comparative experiment.

5) ORE DEPOSITS

There are four types of copper minerals in the target area, including volcanic type, skarn type, hydrothermal type and porphyry type. All the known deposits are viewed as positive samples.

III. RESEARCH APPROACH

A. OVERVIEW

The core component of deep learning is DNN with different structures and hyperparameters [29]. We discuss how to design an approach combining deep learning and geological knowledge to alleviate the problems of sample imbalance and multi-class prediction of mineral resources in the process of deep learning. Fig. 2 shows the main process of our designed approach, which consists of three main steps, described as follows:

- Step 1: We employ ArcGIS software for data preprocessing and GCAE for data augmentation. The spatial datasets containing primary and derived geological, geochemical and geophysical data are established. In addition to common computer vision data augmentation approaches, the geochemical data are trained by GCAE, and the data with abnormal reconstruction errors are augmented and added to the training data as positive samples.

[2]https://www.nanjing.gov.cn/zjnj/zrzk/

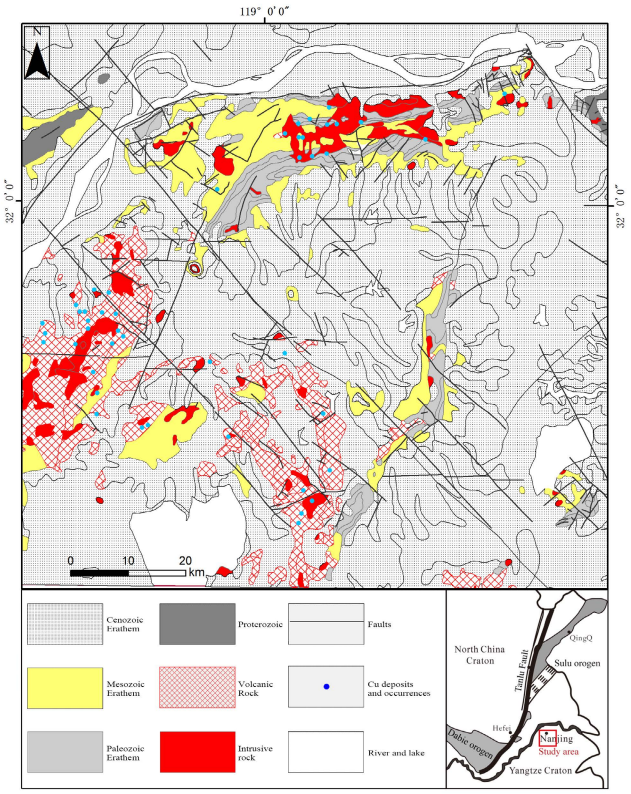

FIGURE 1. Simplified geological map of the target area.

- Step 2: We design and train the Geo-Rnet model for mineral resources prediction. Firstly, we design and optimize network structure and the loss function. Secondly, we select non-repetitive samples in the training data and train Geo-Rnet with them until the number of training times reaches the specified maximum number. In the training process, the samples weight or classification threshold are adjusted based on the loss function to meet the need of imbalanced data classification of mineral resources. The approach increases the model's sensitivity to fault classification and impact of the geological knowledge on the model. Finally, the distribution of mineral resources is predicted in the target area.
- Step 3: We compare the Geo-Rnet model with other popular DNNs for iterative testing, and verify whether the accuracy of the model is improved by combining various channels. If the accuracy of the model improves, the model will be used to generate the MPM; otherwise we will repeat the sample selection and training process.

The multi-channel geoscience data are featured by a large volume of known and unknown ore occurrences, and uneven distribution of samples in the target area. In order to solve the problem that neural network prediction results tend to be one class with too many data samples due to sample imbalance, the loss function is improved. Theoretically, employing the improved loss function and combining multiple indicators for evaluation can more effectively solve the above problems.

Algorithm 1 Procedure of Geo-Rnet Training

Require:
Input: *DATA*: Pretreated multi-channel dataset,
Geo-Rnet: Model based on ResNet after network structure adjustment,
NumTraining: Maximum number of iterations for training
Initialize: θ_G: The initial parameters of *Geo-Rnet*,
num_iterations=0, η=0.001, γ=2, P=0
Ensure:
Save: θ_G^*: The optimal parameters of *Geo-Rnet*

1: *TrainSet*, *TestSet* = Divide(*DATA*); ▷ Divide the training dataset and the test dataset
2: Calculate the number of Class-i samples x_i and the number of all samples $sum = \sum_{i=1}^{n} x_i$ in *TrainSet*;
3: Calculate the weight of all types of samples $\alpha_i = \frac{sum - x_i}{\sum_{i=1}^{n}(sum - x_i)}$ according to (3);
4: **repeat**
5: **while** *num_iterations*<*NumTraining* **do**
6: **for** $i = 1$ **to** $\lceil Length(TrainSet)/m \rceil$ **do**
7: Select m samples $\{(x_1, y_1), (x_2, y_2), \ldots, (x_m, y_m)\}$ from *TrainSet* without repetition;
8: Calculate the loss based on the loss function L_{f1} according to formula(2): $L_{f1} = \frac{1}{m}\sum_{j=1}^{m}\left(-\alpha_i \times \left(1-\hat{p}\right)^{\gamma} \times q \times log\hat{p}\right)$ through forward propagation;
9: Update θ_G^* through back propagation: $\theta_G^* \leftarrow \theta_G - \eta \nabla L_{f1}(\theta_G)$;
10: **end for**
11: Test the new model with obtained parameters in *TestSet* to evaluate the performance and get a new accuracy P;
12: **if** P improves **then**
13: Save θ_G^*;
14: **end if**
15: *num_iterations* = *num_iterations*+1;
16: **end while**
17: **until** *stopping criterion*

The main procedure of the Geo-Rnet approach is shown in Algorithm 1. We use the *DATA* data which is formed by a multi-channel geoscience data after data augmentation and other preprocessing operations to train the network. The dataset is divided into a training dataset *TrainSet* and a test dataset *TestSet* according to the ratio of 7:3 (Line 1). The weight α_i of each class of sample in the loss function is determined by using the amount of data in *TrainSet* (Lines 2-3). During each iteration (Lines 4-5), we pick m samples (Line 7) from *TrainSet* and use them to train the model to get the loss value (Line 8), and then update the model parameters θ_G^* (Line 9) through backpropagation. After updating the model parameters each time, we use them to test in *TestSet*. We observe its accuracy P in *TestSet* (Line 11). If the accuracy

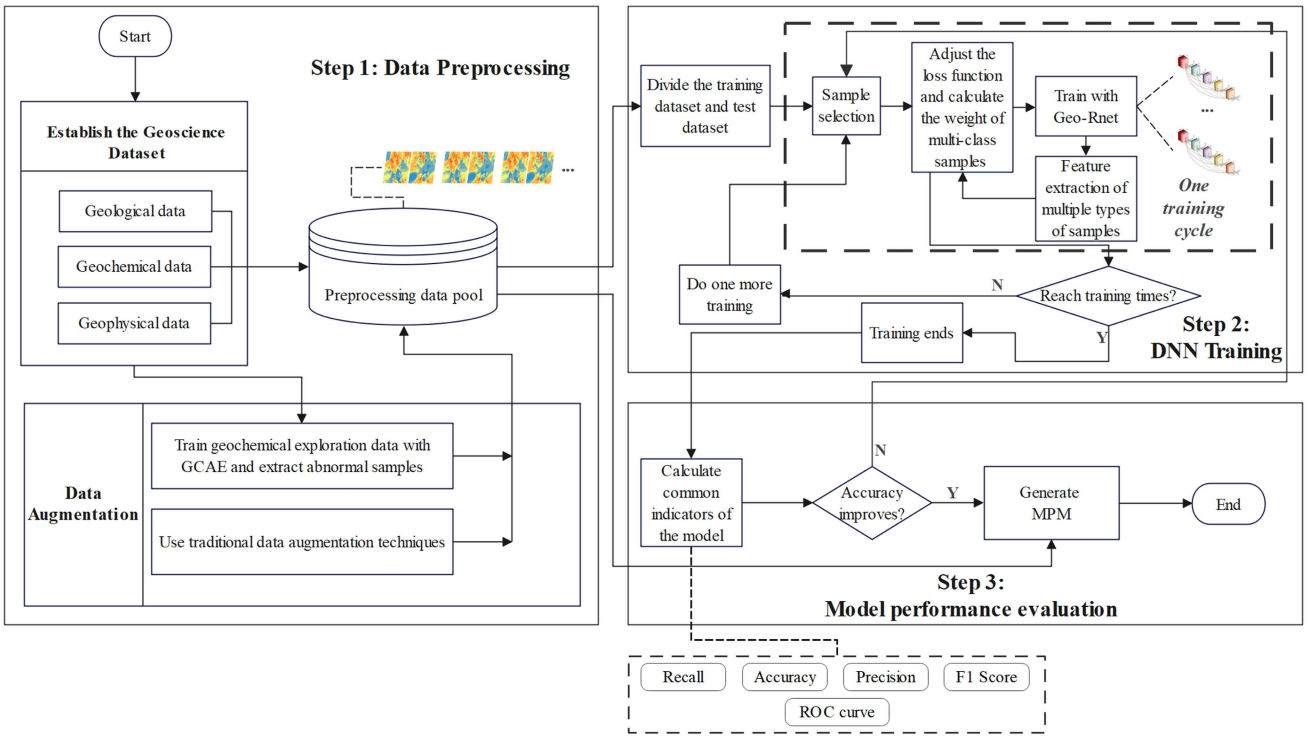

FIGURE 2. Research approach.

improves, then we will save the model parameters for this training (Line 13), and proceed to the next iteration (Line 15).

B. GCAE DESIGN

GCAE is constructed upon an optimized the convolutional autoencoder (CAE) and trained by geochemical data from a multi-channel dataset. The design mainly includes:

1) A DNN is used to construct an encoder q_Φ with Φ as training parameters. The encoder generates an i-dimensional mean vector $M = [\mu_1, \mu_2, \ldots, \mu_i]$ and an i-dimensional standard deviation vector $N = [\sigma_1, \sigma_2, \ldots, \sigma_i]$ by variational inference, from which a mixed Gaussian distribution $q_\Phi(z|X)$ can be represented for approximating the probability distribution z in the hidden space. A random sample is then taken over the distribution $q_\Phi(z|X)$ to generate an implied feature vector $\gamma = M + eps \times e^{\frac{N}{2}}$ of geochemical data, where eps is an i-dimensional random number vector with mean 0 and variance 1.
2) We construct a decoder p_θ with DNN, θ being the training parameters. The role of the decoder is to generate the data $\hat{X} = [\hat{x_1}, \hat{x_2}, \ldots, \hat{x_n}]$, $\hat{x_a} \in (0, 1)$, $a = 1, 2, \ldots, n$ with the implicit feature vector γ and make $\hat{X}$ as similar to X as possible.
3) To make the distribution $q_\Phi(z|X)$ obtained by the encoder q_Φ approximate the probability distribution z and to improve the chance that the decoder p_θ reconstructs the implied feature vector γ as the geochemical data X, we construct the loss function: $L = -\frac{1}{n}\sum_{a=1}^{n}\left(\hat{x_a} \times logx_a + \left(1 - \hat{x_a}\right) \times log\left(1 - x_a\right)\right) + \frac{1}{2}\sum_{b=1}^{i}\left(e^{\sigma_b} + {\mu_b}^2 - 1 - \sigma_b\right)$.
4) We train the encoder q_Φ and the decoder p_θ with the objective of minimizing the loss function.
5) After training, if the value of the reconstructed cross-entropy $\varepsilon = -\frac{1}{n}\sum_{a=1}^{n}(\hat{x_a} \times logx_a + \left(1 - \hat{x_a}\right) \times log\left(1 - x_a\right))$ of a region is lower than the average value, it means that the data in that region have a smaller chance of being reconstructed and the spatial data characteristics are also different from the surrounding region, which is regarded as a geochemical anomaly sample.
6) We add anomalous samples to the training dataset.

C. GEO-RNET DESIGN

During the learning process, the increasing number of network layers often leads to high computing resource consumption, model overfitting, and gradient disappearance or gradient explosion [31]. As the number of network layers increases, continuing to increase the number of layers cannot improve its performance. Instead, there will be significant degradation, which is manifested in the fact that the recognition accuracy of the neural network to the test set and the training set decreases with the increase of the network depth. When the number of network layers is increased initially, the loss of the training set gradually decreases and then tends to be saturated. At this time, if the network depth is

TABLE 1. Geo-Rnet-A Network.

Geo-Rnet-A			
Layer name	Output size	Geochemical/13	Geochemical/42
conv1	114 × 114	13, 128, 5×5, stride 2	42, 128, 5×5, stride 2
conv2_x	58×58	3×3 average pool, stride 2	
		$\begin{bmatrix} 5\times5, & 128 \\ 5\times5, & 128 \end{bmatrix}\times3$	
conv3_x	29 × 29	$\begin{bmatrix} 5\times5, & 256 \\ 5\times5, & 256 \end{bmatrix}\times3$	
conv4_x	15×15	$\begin{bmatrix} 5\times5, & 512 \\ 5\times5, & 512 \end{bmatrix}\times3$	
conv5_x	8×8	$\begin{bmatrix} 5\times5, & 1024 \\ 5\times5, & 1024 \end{bmatrix}\times3$	
	1×1	average pool, 5-d fc, softmax	

TABLE 2. Geo-Rnet-B Network.

Geo-Rnet-B			
Layer name	Output size	Geochemical/13	Geochemical/42
conv1	114 × 114	13, 128, 5×5, stride 2	42, 128, 5×5, stride 2
conv2_x	58×58	3×3 average pool, stride 2	
		$\begin{bmatrix} 5\times5, & 128 \\ 5\times5, & 128 \end{bmatrix}\times2$	
conv3_x	29 × 29	$\begin{bmatrix} 5\times5, & 256 \\ 5\times5, & 256 \end{bmatrix}\times6$	
conv4_x	15×15	$\begin{bmatrix} 5\times5, & 512 \\ 5\times5, & 512 \end{bmatrix}\times8$	
conv5_x	8×8	$\begin{bmatrix} 5\times5, & 1024 \\ 5\times5, & 1024 \end{bmatrix}\times2$	
	1×1	average pool, 5-d fc, softmax	

TABLE 3. Geo-Rnet-C Network.

Geo-Rnet-C			
Layer name	Output size	Geochemical/13	Geochemical/42
conv1	114 × 114	13, 128, 5×5, stride 2	42, 128, 5×5, stride 2
conv2_x	58×58	3×3 average pool, stride 2	
		$\begin{bmatrix} 1\times1, & 128 \\ 5\times5, & 128 \\ 1\times1, & 512 \end{bmatrix}\times2$	
conv3_x	29 × 29	$\begin{bmatrix} 1\times1, & 256 \\ 5\times5, & 256 \\ 1\times1, & 1024 \end{bmatrix}\times6$	
conv4_x	15×15	$\begin{bmatrix} 1\times1, & 512 \\ 5\times5, & 512 \\ 1\times1, & 2048 \end{bmatrix}\times8$	
conv5_x	8×8	$\begin{bmatrix} 1\times1, & 1024 \\ 5\times5, & 1024 \\ 1\times1, & 4096 \end{bmatrix}\times2$	
	1×1	average pool, 5-d fc, softmax	

further increased, the loss of the training set will increase, and the accuracy of the model will decrease instead of rising. [27] proposed the residual module, which can effectively avoid the problem of vanishing network gradient and gradient explosion caused by DNN deepening. A residual network is composed of several stacked residual blocks, where a residual block comprises several network layers and a shortcut link. If the input of the residual block is x, and the output of x after several convolutional layers is $F(x)$, then the output of the entire residual block is $F(x)+x$. Quick links of residual block are the core of the residual network, which solve the problem of gradient disappeared within DNN. At the same time, the direct backward propagation of shallow network features is combined with the deep nonlinear features in the network, and the final feature vectors obtained can better reflect the nature of short-term timing than the feature vectors extracted by ordinary convolution. Moreover, the shallow temporal features extracted above can be reused [27], [32].

The training datasets of the model are derived from Section II Part B, which are divided into 13 data channels composed of rock mass, fault, geophysics and 10 main geochemical elements, and 42 data channels composed of rock mass, fault, geophysics and 39 geochemical elements. The datasets input of neural network is 224 × 224 × 13 and 224 × 224 × 42, respectively. Their network architecture is shown in Table 1, Table 2 and Table 3. The overview structure of Geo-Rnet is shown in Fig. 3, and the structure diagrams of Geo-Rnet-A, Geo-Rnet-B and Geo-Rnet-C are shown in Fig. 4, Fig. 5 and Fig. 6, respectively.

In the field of image classification, the most commonly used cross entropy loss function (CrossEntropy) is defined as (1):

$$L_{ce} = -q log\left(\hat{p}\right). \tag{1}$$

where q is the actual category vector and $\hat{p}$ is the predicted category vector given by the model. $\hat{p}$ reflects the confidence level of the model in determining the input image as the true category q. A larger $\hat{p}$ indicates that the classification is more accurate, representing that the samples are easy to distinguish, and the corresponding loss L_{ce} is smaller. A smaller $\hat{p}$ means the lower confidence level of the classification, representing that the samples are harder to classify, and the corresponding loss L_{ce} is larger. For a dataset with uniformly distributed samples, training the model by the cross-entropy loss function often yields good classification results. However, when the sample distribution is imbalanced, the distribution of the loss function L_{ce} is skewed, and if a certain class of samples accounts for a much larger proportion of the entire dataset than other classes of samples, the samples with the larger proportion will dominate the loss function.

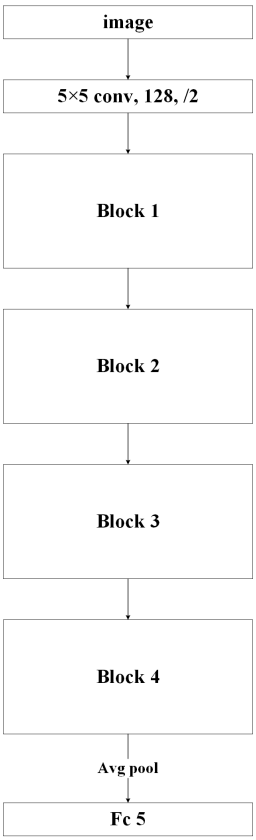

FIGURE 3. The overview structure of Geo-Rnet.

Due to the skewing of the loss function, the model training process will favor the category with more samples, resulting in poorer performance of the model for the category with fewer samples [33].

We consider four types of mineral resources samples in this paper. The numbers of samples among the various types are unbalanced in the target area. The traditional cross-entropy loss function cannot effectively solve the problem of imbalanced samples. The categories with a smaller number of samples receive less attention in the model training process, thus failing to obtain the correct classification results.

We employ the focal loss function [34] to set the weight of each sample category and thus effectively balance the weight of each category on the total loss. The focal loss function can balance the distribution of the loss function by increasing the weights of a few categories in the loss function, thus solving the problem of category imbalance and eliminating the need to compute complex weight mappings. In this regard, the model can better capture the signal features. The focal loss function is defined in (2):

$$L_{f1} = -\alpha \times \left(1 - \hat{p}\right)^{\gamma} \times q \times log\hat{p}. \tag{2}$$

where q is the actual category vector and $\hat{p}$ is the predicted category vector given by the model. $\gamma > 0$ is an adjustable parameter that adaptively adjusts the rate at which samples are weighted down. $\hat{p}$ converges to 1 and $\left(1 - \hat{p}\right)^{\gamma}$ converges to 0 for easily distinguished samples, and $\hat{p}$ converges to 0 and $\left(1 - \hat{p}\right)^{\gamma}$ converges to 1 for more difficult samples. It can be observed that the value of focal loss does not change for inaccurately classified samples, and becomes smaller for accurately classified samples. Overall, it is equivalent to increasing the weight of inaccurately classified samples in the loss function, making the model focus more on the less distinguishable samples and reducing the influence of easily distinguishable samples. Let α denote the respective weight of each class of samples. Assuming that there are n classes of samples, the total number of samples of class i is x_i, the total number of all samples is $sum = \sum_{i=1}^{n} x_i$, and the weight α_i of each class of samples are calculated according to (3) as follows:

$$\alpha_i = \frac{sum - x_i}{\sum_{i=1}^{n} (sum - x_i)}. \tag{3}$$

In this project, the weight of each sample is calculated from (3), which is 0.238 for hydrothermal ore type, 0.240 for porphyry ore type, 0.218 for skarn ore type, and 0.179 for volcanic ore type. By setting different weights to adapt to the demand of multiple classifications of imbalanced data of mineral resources, the sensitivity of misclassification is enhanced, and the constraint of geological knowledge on the model is strengthened.

IV. RESULT AND DISCUSSION

We design a series of experiments to evaluate the effectiveness of the Geo-Rnet approach for mineral prediction in the target area. The first is to evaluate the impact of data augmentation and loss function adjustment on the classification performance. Secondly, we evaluate the impact of different network architectures and the number of data channels on Geo-Rnet. Thirdly, the performance of Geo-Rnet is compared with a variety of popular DNNs. Finally, we use Geo-Rnet to make multi-class prediction of copper minerals in the target area.

For all the DNNs participating in the comparison, we adopt Adam momentum optimizer, with a learning rate of 0.001, a weight decay of 5×10^{-4}, and a training iteration number of 100. The same dataset is used for training and verification.

For performance evaluation and comparison, we use six different indicators, including accuracy, precision, recall, F1 Score and ROC curve [3], [11], [19], [24], [35], [36]. Among them, accuracy is the proportion of the number of correctly classified sample in the total number of samples. Precision is for our prediction results, which is the ratio of the predicted positive samples to all positive samples. Recall is for our original sample, which measures the percentage of positive examples in the datasets that are predicted to be true. F1 Score can be regarded as a weighted average of model precision and recall. The ROC curve can detect the identification ability of performance at any threshold value. The closer the ROC curve is to the upper left corner, the higher the accuracy of the model. The point closest to the upper left corner of

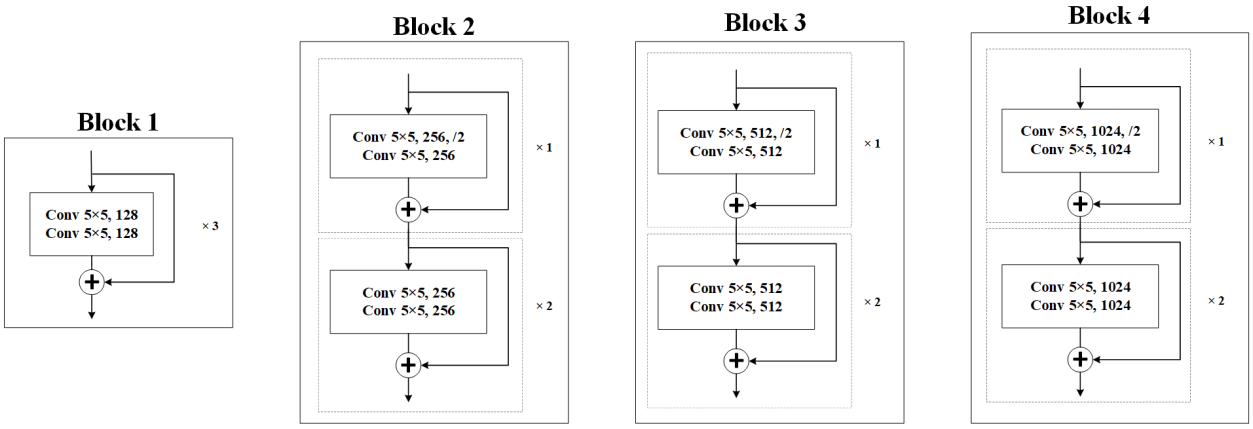

FIGURE 4. The structure diagrams of Geo-Rnet-A.

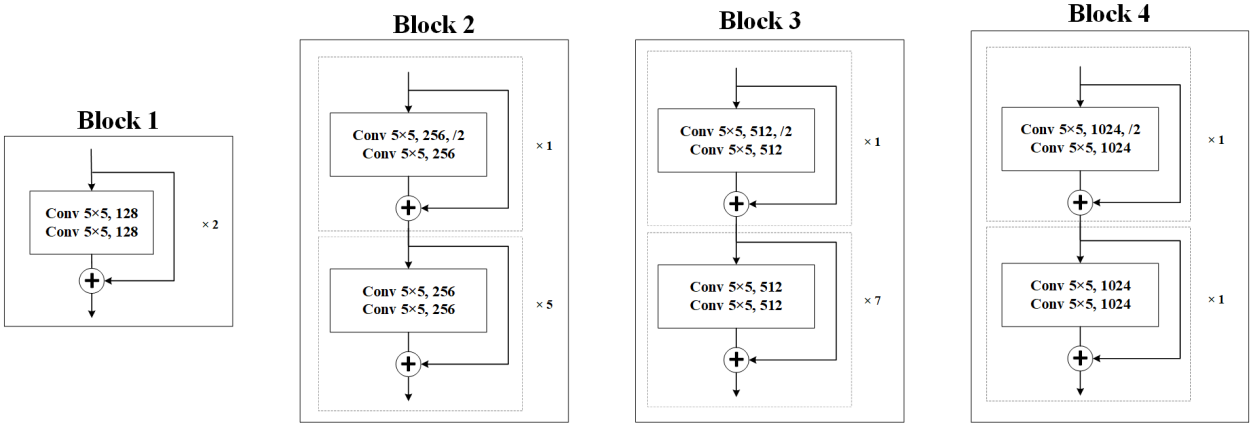

FIGURE 5. The structure diagrams of Geo-Rnet-B.

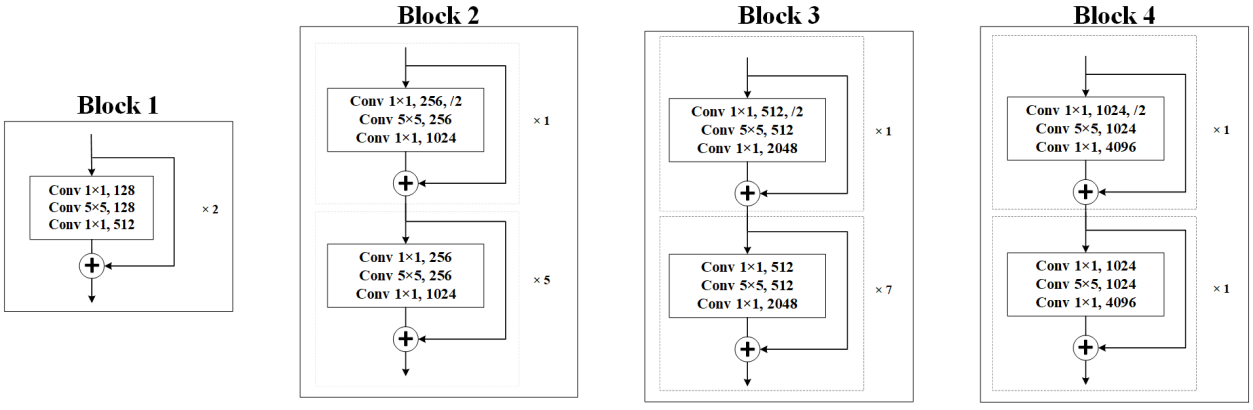

FIGURE 6. The structure diagrams of Geo-Rnet-C.

the ROC curve is the best threshold with the least errors. Meanwhile, the total number of false positives and false negatives are the least. The macro-averaged precision, recall and F1 scores are computed using the arithmetic mean of all the per-class precision, recall and F1 scores. The micro averaging computes a global average precision, recall and F1 scores by counting the sums of the True Positives (TP), False Negatives (FN), and False Positives (FP).

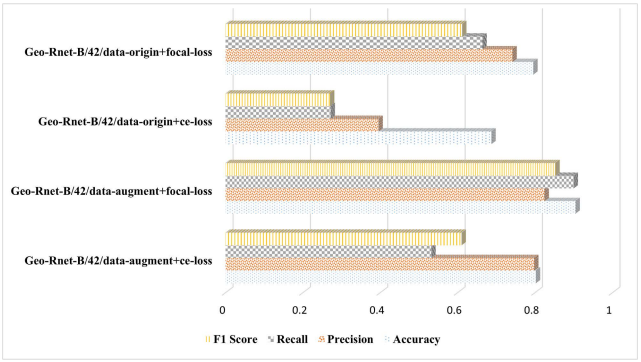

FIGURE 7. F1 Score, recall, precision and accuracy results obtained by the first experiment.

A. EXPERIMENT 1: ADJUST THE IMPACT OF DATA AUGMENTATION AND LOSS FUNCTIONS

There are 46 known copper deposits of various types in the target area, including 4 hydrothermal deposits, 3 porphyry deposits, 12 skarn deposits and 27 volcanic deposits. The minimum grid cell of 10×10 pixel(at 100m per pixel) will be set for the target area. According to the features of geological data, in order to maintain the consistency of spatial attributes and increase the number of positive samples, the grid cells around the positive samples are trained as positive samples. In the end, there are a total of 10823 samples in the target area, 351 of which are positive samples and the remaining 10472 are non-positive samples. The samples are divided into a training set and a test set according to the ratio of 7:3. There are 246 positive samples in the training set and 7331 non-positive samples[3] in the training set. There are 105 positive samples in the test set and 3141 non-positive samples in the test set. Data channels are divided into 42 data channels and 13 data channels as described in the preceding sections.

In order to alleviate the imbalance of positive and negative samples, 370 samples in line with geological cognition are augmented by GCAE, and 866 samples are augmented by Gaussian noise and salt and pepper noise. Finally, a total of 1482 positive samples participated in the training. For the non-positive samples, 5831 samples are randomly discarded in the space far away from the positive samples in the target area, and about 1500 non-positive samples are obtained.

From the comparison results of Geo-Rnet-A, Geo-Rnet-B and Geo-Rnet-C (in Fig. 14), it can be seen that Geo-Rnet-B achieves the best comprehensive performance. Thus, we select Geo-Rnet-B as the test network, and 42 data channels are used as experimental data. Then we design four candidate schemes for experiments: original data and focal loss function, original data and cross-entropy loss function, augmented data and focal loss function, and augmented data and cross-entropy loss function. The final experimental results are shown in Fig. 7 and Fig. 8.

[3]We use non-positive samples to replace negative samples. The reason is that negative samples in this study do not mean they do not contain mineral resources, since the size of the survey data is too small to judge.

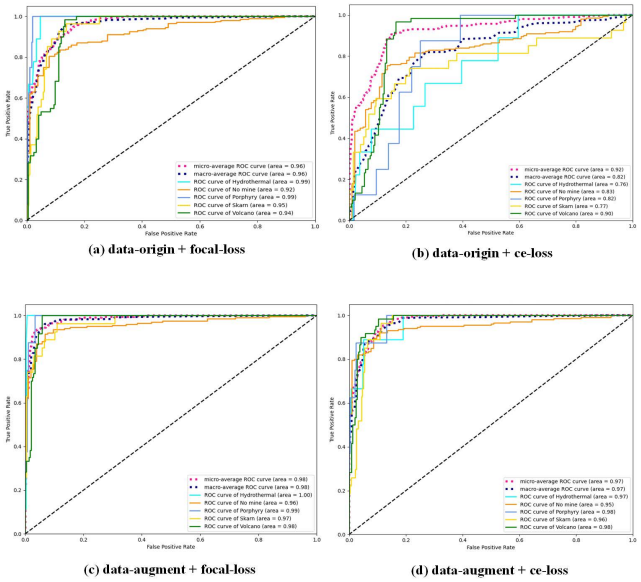

FIGURE 8. ROC results obtained by the first experiment.

It can be seen from Fig. 7 that the training result of the improved focal loss function is better than that of the traditional cross-entropy loss function, both in the original data and augmented data. Especially under the original data, compared with the cross-entropy loss function, the focal loss function improves the accuracy by 15.78%, the precision by 87.56%, the recall by 114.35%, and the F1 Score by 126.46%. With the significant improvement of F1 Score, it validates that the use of focal loss function can effectively solve the problem of uneven distribution among samples and effectively overcome the probability skew of neural network to no mining area. Under the same loss function, the performance of the network is also greatly improved after data augmentation. Especially under the cross-entropy loss function, compared with the original data, the data augmentation improves the accuracy by 16.74%, the precision by 101.77%, the recall by 95.81%, and the F1 Score by 125.91%, indicating that the neural network pays more attention to the ore deposits after the data augmentation. In Fig. 8, we can see that the model trained with the augmented data and focal loss function achieves better performance, since the areas occupied by its macro and micro ROC curves are larger than those obtained by the other schemes. The worst results are obtained from the model trained using the original data and the traditional cross-entropy loss function.

We used the model trained by the above four schemes to predict minerals in the target area. The results are shown in Fig. 9. By analyzing Fig. 9 (c) and (d), we find that the network trained under the original data and cross-entropy loss function overfits the mineral prediction of the target area. However, the network trained on augmented data and cross-entropy loss function alleviates the problem of overfitting, yet the predicted mineral distribution is still around the known mineral sites, and the generalization ability is poor. It can be

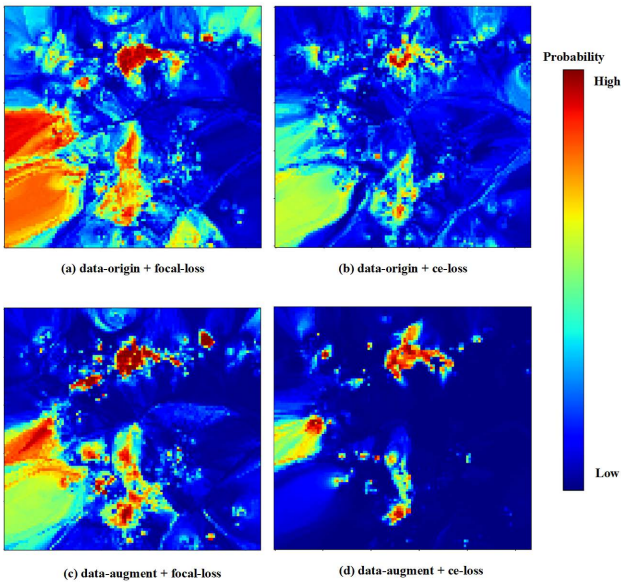

FIGURE 9. MPM results obtained by the first experiment.

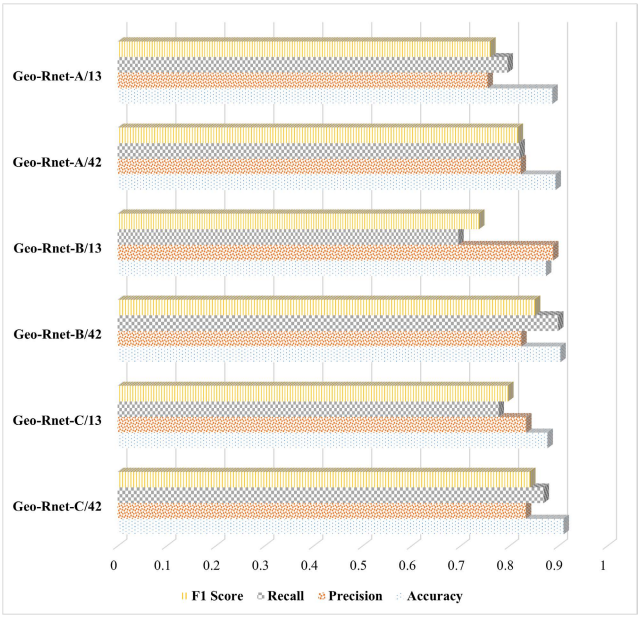

FIGURE 10. F1 Score, recall, precision and accuracy results obtained by the second experiment.

concluded that the network trained under the augmented data and focal loss function improves generalization ability and the prediction results are more accurate than those of the other schemes.

B. EXPERIMENT 2: ADJUST THE IMPACT OF DIFFERENT NETWORK DEPTHS AND NUMBER OF DATA CHANNELS

From Experiment 1, it is found that the neural network trained with augmented data and focal loss function achieves better results than the other schemes. In the second experiment, we evaluate the effect of different network depths and data channels on the model training results. In this experiment, the schemes of augmentation data and focal loss function are used to train the neural networks participating in the comparison, which are Geo-Rnet-A, Geo-Rnet-B and Geo-Rnet-C, with 13 and 42 data channels, respectively. Experimental results are shown in Fig. 10 and Fig. 11.

It can be seen from Fig. 10 that, under the same network structure, the model trained with 42 data channels has a slight advantage over the model trained with the 13 data channels in accuracy, recall and F1 Score, yet the precision is in an uncertain state. When the three networks with different depths are trained with 42 data channels, the performance of the Geo-Rnet-A is worse than that of the other two networks in the four scores, and Geo-Rnet-B is slightly superior in accuracy and precision compared with Geo-Rnet-C. The three networks with different depths have their own advantages and disadvantages when they all use 13 data channels for training, but Geo-Rnet-A has higher accuracy. From Fig. 11, we can see that the macro ROC value of the model trained with 42 data channels on the test set is 1% higher than that of the model trained with 13 data channels. However, the micro ROC value of the two models is almost the same. In addition, in the case of the same number of channels, the results obtained by the

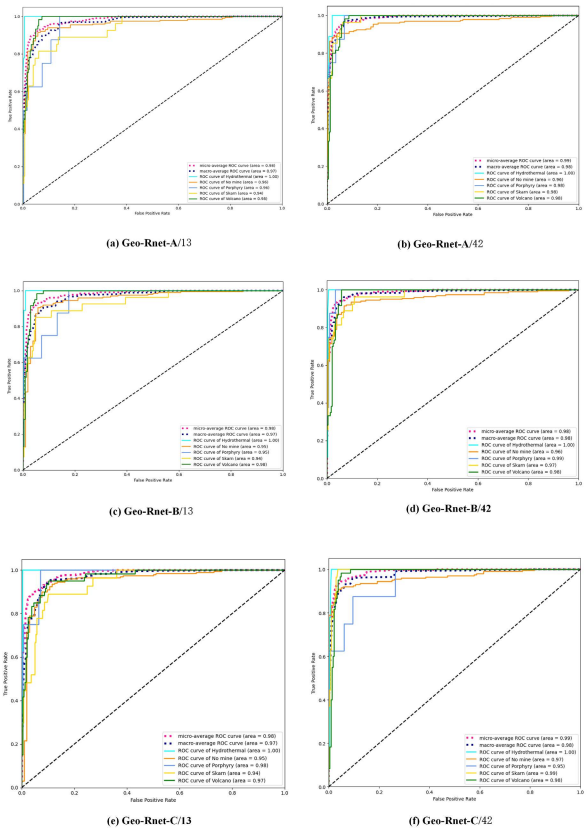

FIGURE 11. ROC results obtained by the second experiment.

network with different depths are roughly the same. These experimental results show that, in the case of higher data channels, increasing the network depth may pose a positive

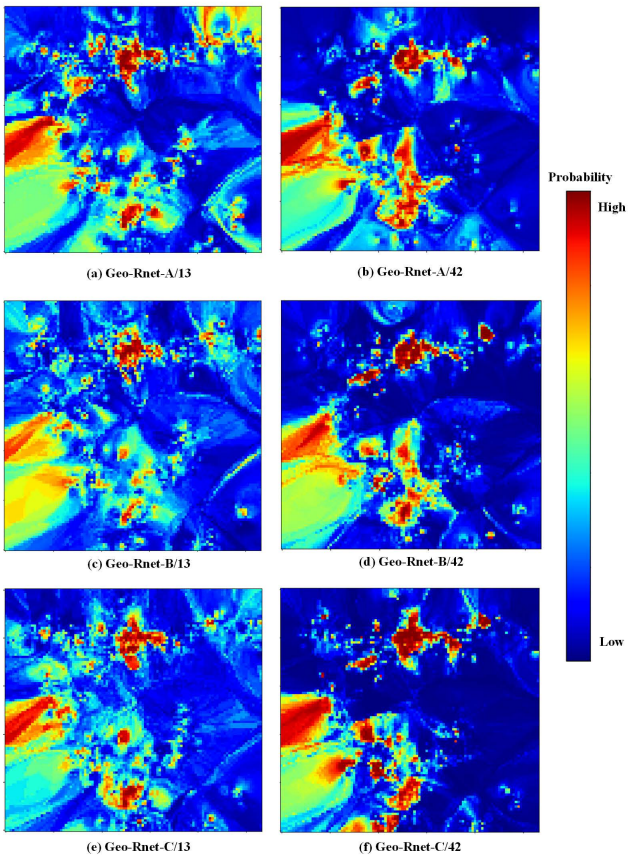

FIGURE 12. MPM results obtained by the second experiment.

impact on the results, whereas in the case of lower data channels, the change of network depth has little effect on the results.

We use different network depths and different data channels during training to generate MPM. The results are shown in Fig. 12. Interestingly, only Geo-Rnet-A has high metallogenic prediction probability for the north area with 13 data channels, whereas the three networks with different depths have roughly the same regional metallogenic prediction probability for the south area with 42 data channels.

C. EXPERIMENT 3:ADJUST THE IMPACT OF DIFFERENT DNNs

According to the results of Experiment 2, our improved network with 42 data channels shows better performance than those with 13 data channels. In this section, we consider that some DNNs and their improved versions have little difference in network structure and performance, so we select the currently mainstream DNNs (NiN [37], InceptionV3 [38], AlexNet [39], Densenet121 [40], VGG16 and VGG11 [41]) to compare with our improved DNNs (Geo-Rnet-A, Geo-Rnet-B and Geo-Rnet-C). In this experiment, 42 data channels were used, and all of them are trained under the training scheme with augmented data and focal loss function. The experimental results are shown in Fig. 13 and Fig. 14.

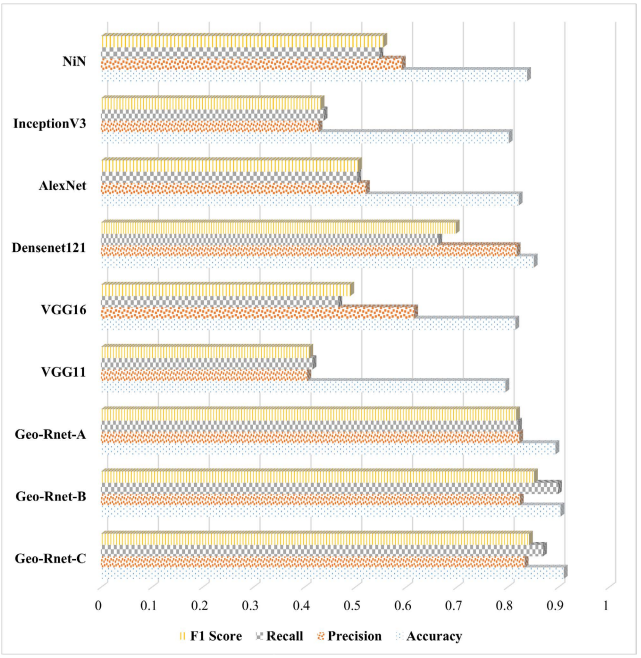

FIGURE 13. F1 Score, recall, precision and accuracy results obtained by the third experiment.

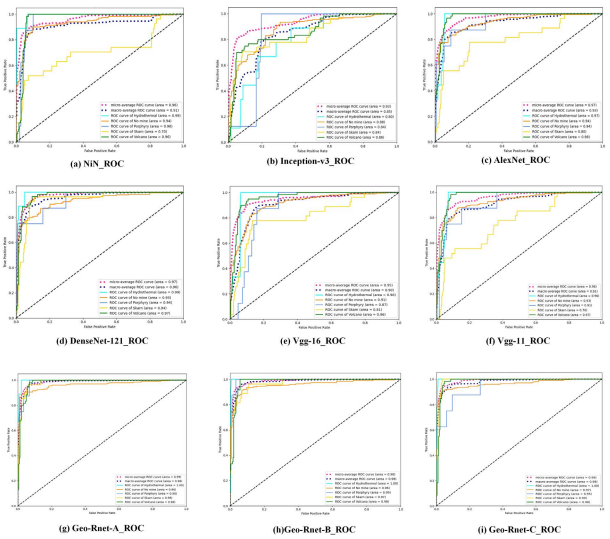

FIGURE 14. ROC results obtained by the third experiment.

As shown in Fig. 13, the performance of our improved network in this task is significantly better than that of the others. Among them, Densenet121 achieves the second highest accuracy and precision next to Geo-Rnet, but its recall and F1 Score are unpromising. The performance of VGG11 is the worst among all the candidate networks, which may be restricted by its shallow network structure, leading to its low performance in deep learning tasks. It can be seen from Fig. 14 that the ROC curve results of our network Geo-Rnet-A, Geo-Rnet-B and Geo-Rnet-C are better than

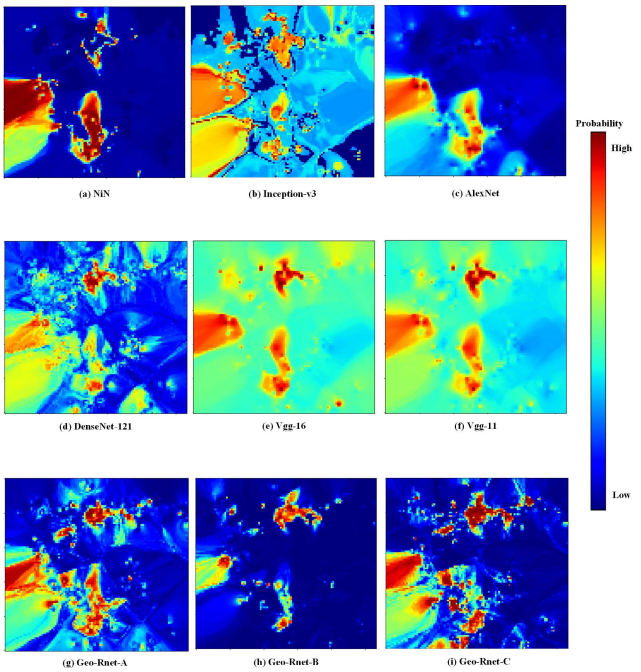

FIGURE 15. MPM results obtained by the third experiment.

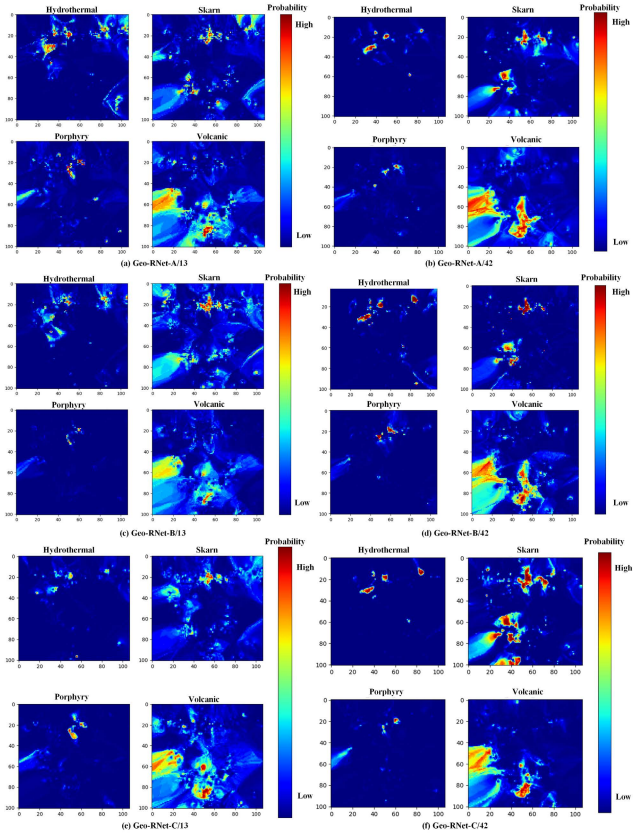

FIGURE 16. Multi-class prediction results by Geo-Rnet.

the others. The MPM generated by the above nine networks is shown in Fig. 15.

The experimental results in Fig. 15 show that the prediction results of VGG16 and VGG11 are roughly the same and have distinct differences with that of the others. The prediction results of AlexNet for the north area are incomplete, indicating the limited capability of the model in learning the complex data features of mineral resources. The prediction results of NiN network and Densenet121 are the closest to those of our improved networks, whereas the results of InceptionV3 are quite different.

D. EXPERIMENT 4: GEO-RNET IS USED FOR MULTI-CLASS PREDICTION OF MINERAL RESOURCES

By observing the above experimental results, we can see that our proposed Geo-Rnet model achieves better performance than the popular DNN models in all the indicators. In this section, we will use Geo-Rnet to make multi-class prediction and analyze the results of mineral resources in the research area. The experiment is still carried out according to the focal loss function and data augmentation scheme. Geo-Rnet-A, Geo-Rnet-B and Geo-Rnet-C are used for training with 13 and 42 data channels respectively.

As shown in Fig. 16, we can see that most of the hydrothermal, skarn and porphyry copper deposits are in the north of the target area and a small part is in the south of the target area, while the volcanic copper deposits are concentrated in the southwest of the target area, which is consistent with the current geological survey results of the target area introduced in Section II. The left panel of Fig. 16 shows the prediction results obtained by Geo-Rnet model trained with 13 data channels. It can be seen that the overall distribution of mineral resources is sparse, and the potential mineral areas are not obvious. The right panel of Fig. 16 shows the prediction results obtained by Geo-Rnet trained with 42 data channels. We can see that the results are more in line with the geological survey result, with less divergence and more concentrated in the places with high probability of metallogenic prediction. It can be concluded that more channels of geoscience data have a great impact on the prediction results.

V. CONCLUSION

We design and implement Geo-Rnet and GCAE for multi-class prediction of mineral resources. Firstly, we use the GCAE to find the abnormal information in the original data distribution under the black-box condition and augment the abnormal data. Secondly, network structure and the loss function are designed in Geo-Rnet to improve analytical accuracy and the constraint of geological knowledge on the model. Finally, by comparing Geo-Rnet with other popular DNNs through a series of experiments, it is proved that Geo-Rnet improves the accuracy of multi-class prediction of mineral resources. In addition, we use Geo-Rnet to conduct multi-class prediction of copper mines in the target area. Geo-Rnet achieves average prediction accuracy of 91.11% and about 89.98% of known mineralization points are located in the predicted areas. Our research provides a new potential approach

for mineral prospectivity in the target area. However, because the formation of mineral resources is a small probability event with very few samples, there are still great challenges in mineral resource prediction based on deep learning. In the future, We plan to develop more advanced models with better prediction performance.

DECLARATION OF COMPETING INTEREST

The authors declare that they have no known competing financial interests or personal relationships that could have appeared to influence the work reported in this paper.

REFERENCES

[1] P. Zhao, "Characteristics and rational utilization of geological big data," *Earth Sci. Frontiers*, vol. 26, no. 4, p. 1, Jul. 2019.

[2] R. B. Taylor and T. A. Steven, "Definition of mineral resource potential," *Econ. Geol.*, vol. 78, no. 6, pp. 1268–1270, Oct. 1983.

[3] J. Li, P. A. Cawood, L. Ratschbacher, Y. Zhang, S. Dong, Y. Xin, H. Yang, and P. Zhang, "Building Southeast China in the late Mesozoic: Insights from alternating episodes of shortening and extension along the Lianhuashan fault zone," *Earth-Sci. Rev.*, vol. 201, Feb. 2020, Art. no. 103056.

[4] M. Yousefi, O. P. Kreuzer, V. Nykänen, and J. M. A. Hronsky, "Exploration information systems—A proposal for the future use of GIS in mineral exploration targeting," *Ore Geol. Rev.*, vol. 111, Aug. 2019, Art. no. 103005.

[5] O. Maas, "Seasonal contrast: Unsupervised pre-training from uncurated remote sensing data," in *Proc. IEEE/CVF Int. Conf. Comput. Vis.*, Jun. 2021, pp. 9414–9423.

[6] Q.-M. Cheng, "Application of a newly developed boost weights of evidence model(BoostWofE) for mineral resources quantitative assessments," *J. Jilin Univ., Earth Sci. Ed.*, vol. 42, no. 6, pp. 1976–1985, 2012.

[7] G. Markus, "Deep learning and process understanding for data-driven Earth system science," *Nature*, vol. 599, pp. 195–204, Feb. 2019.

[8] T. Niiranen, V. Nykänen, and I. Lahti, "Scalability of the mineral prospectivity modelling—An orogenic gold case study from northern Finland," *Ore Geol. Rev.*, vol. 109, pp. 11–25, Jun. 2019.

[9] O. P. Kreuzer, M. Yousefi, and V. Nykänen, "Introduction to the special issue on spatial modelling and analysis of ore-forming processes in mineral exploration targeting," *Ore Geol. Rev.*, vol. 119, Apr. 2020, Art. no. 103391.

[10] J. Granek and E. Haber, "Data mining for real mining: A robust algorithm for prospectivity mapping with uncertainties," in *Proc. SIAM Int. Conf. Data Mining*. Philadelphia, PA, USA: SIAM, Jun. 2015, pp. 145–153.

[11] Y. Xu, Z. Li, Z. Xie, H. Cai, P. Niu, and H. Liu, "Mineral prospectivity mapping by deep learning method in Yawan-Daqiao area, Gansu," *Ore Geol. Rev.*, vol. 138, Nov. 2021, Art. no. 104316.

[12] H. Li, X. Li, F. Yuan, S. M. Jowitt, M. Zhang, J. Zhou, T. Zhou, X. Li, C. Ge, and B. Wu, "Convolutional neural network and transfer learning based mineral prospectivity modeling for geochemical exploration of Au mineralization within the Guandian–Zhangbaling area, Anhui province, China," *Appl. Geochem.*, vol. 122, Nov. 2020, Art. no. 104747.

[13] M. Daviran, A. Maghsoudi, R. Ghezelbash, and B. Pradhan, "A new strategy for spatial predictive mapping of mineral prospectivity: Automated hyperparameter tuning of random forest approach," *Comput. Geosci.*, vol. 148, Mar. 2021, Art. no. 104688.

[14] N. Yang, Z. Zhang, J. Yang, Z. Hong, and J. Shi, "A convolutional neural network of GoogLeNet applied in mineral prospectivity prediction based on multi-source geoinformation," *Natural Resour. Res.*, vol. 30, no. 6, pp. 3905–3923, Dec. 2021.

[15] Y. Xiong, R. Zuo, and E. J. M. Carranza, "Mapping mineral prospectivity through big data analytics and a deep learning algorithm," *Ore Geol. Rev.*, vol. 102, pp. 811–817, Nov. 2018.

[16] T. C. McCuaig, S. Beresford, and J. Hronsky, "Translating the mineral systems approach into an effective exploration targeting system," *Ore Geol. Rev.*, vol. 38, no. 3, pp. 128–138, Nov. 2010.

[17] B. Yet, Z. B. Perkins, T. E. Rasmussen, N. R. M. Tai, and D. W. R. Marsh, "Combining data and meta-analysis to build Bayesian networks for clinical decision support," *J. Biomed. Informat.*, vol. 52, pp. 373–385, Dec. 2014.

[18] S. Zhang and K. Xiao, "Random forest-based mineralization prediction of the Lala-type Cu deposit in the Huili area, Sichuan province," *Geol. Explor.*, vol. 56, no. 2, pp. 239–252, 2020.

[19] F. Maepa, R. S. Smith, and A. Tessema, "Support vector machine and artificial neural network modelling of orogenic gold prospectivity mapping in the Swayze greenstone belt, Ontario, Canada," *Ore Geol. Rev.*, vol. 130, Mar. 2021, Art. no. 103968.

[20] A. Porwal, E. J. M. Carranza, and M. Hale, "Bayesian network classifiers for mineral potential mapping," *Comput. Geosci.*, vol. 32, no. 1, pp. 1–16, Feb. 2006.

[21] T. Sun, F. Chen, L. Zhong, W. Liu, and Y. Wang, "GIS-based mineral prospectivity mapping using machine learning methods: A case study from Tongling ore district, eastern China," *Ore Geol. Rev.*, vol. 109, pp. 26–49, Jun. 2019.

[22] T. Sun, H. Li, K. Wu, F. Chen, Z. Zhu, and Z. Hu, "Data-driven predictive modelling of mineral prospectivity using machine learning and deep learning methods: A case study from southern Jiangxi province, China," *Minerals*, vol. 10, no. 2, p. 102, Jan. 2020.

[23] Y. Xiong and R. Zuo, "A positive and unlabeled learning algorithm for mineral prospectivity mapping," *Comput. Geosci.*, vol. 147, Feb. 2021, Art. no. 104667.

[24] C. Zhang, R. Zuo, and Y. Xiong, "Detection of the multivariate geochemical anomalies associated with mineralization using a deep convolutional neural network and a pixel-pair feature method," *Appl. Geochemistry*, vol. 130, Jul. 2021, Art. no. 104994.

[25] S. Zhang, E. J. M. Carranza, K. Xiao, Z. Chen, N. Li, H. Wei, J. Xiang, L. Sun, and Y. Xu, "Geochemically constrained prospectivity mapping aided by unsupervised cluster analysis," *Natural Resources Res.*, vol. 30, no. 3, pp. 1955–1975, Jun. 2021.

[26] S. Zhang, E. J. M. Carranza, H. Wei, K. Xiao, F. Yang, J. Xiang, S. Zhang, and Y. Xu, "Data-driven mineral prospectivity mapping by joint application of unsupervised convolutional auto-encoder network and supervised convolutional neural network," *Natural Resources Res.*, vol. 30, no. 2, pp. 1011–1031, Apr. 2021.

[27] K. He, X. Zhang, S. Ren, and J. Sun, "Deep residual learning for image recognition," in *Proc. IEEE Conf. Comput. Vis. Pattern Recognit. (CVPR)*, Jun. 2016, pp. 770–778.

[28] Z. U. O. Renguang, "Data science-based theory and method of quantitative prediction of mineral resources," *Earth Sci. Frontiers*, vol. 28, no. 3, p. 49, 2021.

[29] H. Wang, "Application of multifractal method to the geochemical exploration of Nanjing-Zhenjiang copper-polymetallic metallogenic belt," *Metal Mine*, vol. 41, no. 12, p. 79, May 2012.

[30] Y. Sun, "The latest Yanshanian magmatic and metallogenic events in the middle-lower Yangtze River belt: Evidence from the Ningzhen region," *Chin. Sci. Bull.*, vol. 34, no. 58, pp. 154–171, 2013.

[31] D. Sarwinda, R. H. Paradisa, A. Bustamam, and P. Anggia, "Deep learning in image classification using residual network (ResNet) variants for detection of colorectal cancer," *Proc. Comput. Sci.*, vol. 179, pp. 423–431, Apr. 2021.

[32] S. Woldegiorgis, A. Enqvist, and J. Baciak, "ResNet and CycleGAN for pulse shape discrimination of He-4 detector pulses: Recovering pulses conventional algorithms fail to label unanimously," *Appl. Radiat. Isot.*, vol. 176, Oct. 2021, Art. no. 109819.

[33] Y. Wang, X. Ma, Z. Chen, Y. Luo, J. Yi, and J. Bailey, "Symmetric cross entropy for robust learning with noisy labels," 2019, *arXiv:1908.06112*.

[34] T. Y. Lin, "Focal loss for dense object detection," *IEEE Trans. Pattern Anal. Mach. Intell.*, vol. 99, pp. 2999–3007, 2017.

[35] A. G. Fabbri and C.-J. Chung, "On blind tests and spatial prediction models," in *Progress in Geomathematics*. Berlin, Germany: Springer, 2008, pp. 315–332.

[36] P. Zhang, B. Ren, H. Dong, and Q. Dai, "CAGFuzz: Coverage-guided adversarial generative fuzzing testing for image-based deep learning systems," *IEEE Trans. Softw. Eng.*, early access, Nov. 2, 2021, doi: 10.1109/TSE.2021.3124006.

[37] M. Lin, Q. Chen, and S. Yan, "Network in network," in *Proc. ICLR*, 2014, pp. 1–10.

[38] C. Szegedy, "Rethinking the inception architecture for computer vision," in *Proc. IEEE Conf. Comput. Vis. Pattern Recognit. (CVPR)*, Aug. 2016, pp. 2818–2826.

[39] A. Krizhevsky, I. Sutskever, and G. E. Hinton, "ImageNet classification with deep convolutional neural networks," *Commun. ACM*, vol. 60, no. 2, pp. 84–90, Jun. 2012, doi: 10.1145/3065386.

[40] G. Huang, Z. Liu, L. Van Der Maaten, and K. Q. Weinberger, "Densely connected convolutional networks," in *Proc. IEEE Conf. Comput. Vis. Pattern Recognit. (CVPR)*, Jul. 2017, pp. 1–15.
[41] K. Simonyan and A. Zisserman, "Very deep convolutional networks for large-scale image recognition," 2014, *arXiv:1409.1556*.

LIANG DING received the M.S. degree from Nanjing Normal University, in 2008, majoring in cartography and geographical information system. He is currently pursuing the Ph.D. degree with the College of Computer and Information, Hohai University, Nanjing, China. His current research interests include machine learning and data mining.

YUELONG ZHU is currently a Professor and a Ph.D. Supervisor with the College of Computer and Information, Hohai University, Nanjing, China. He is also the Deputy Chairperson of the Water Resources Informatization Special Committee of the China Hydraulic Engineering Society, and the Vice Chairperson of the Jiangsu Water Resources Protection Association. His research interests include intelligent information processing and data mining, and water conservancy informatization. He was awarded the National Second Prize for Scientific and Technological Progress, the First Prize for Excellent Achievements of the Ministry of Education, and the Dayu Water Science and Technology First Prize.

PENGCHENG ZHANG (Member, IEEE) received the Ph.D. degree in computer science from Southeast University, in 2010. He is currently a Full Professor with the College of Computer and Information, Hohai University, Nanjing, China. His research interests include software engineering, services computing, and data science. He has published in premiere or famous computer science journals, such as IEEE TRANSACTIONS ON BIG DATA, IEEE TRANSACTIONS ON CLOUD COMPUTING, IEEE TRANSACTIONS ON EMERGING TOPICS IN COMPUTING, IEEE TRANSACTIONS ON SERVICES COMPUTING, IEEE TRANSACTIONS ON SOFTWARE ENGINEERING, IEEE TRANSACTIONS ON KNOWLEDGE AND DATA ENGINEERING, and *ACM Transactions on Data Science*. He was the Co-Chair of IEEE AI Testing 2019 Conference. He served as a technical program committee member on various international conferences.

HAI DONG (Senior Member, IEEE) received the bachelor's degree from Northeastern University, China, and the Ph.D. degree from the Curtin University of Technology, Australia. He is currently a Lecturer at the School of Computing Technologies, RMIT University, Melbourne, Australia. He has published a monograph and over 110 research publications in international journals and conferences, such as *ACM Computing Surveys*, *Communications of the ACM*, IEEE TRANSACTIONS ON CLOUD COMPUTING, IEEE TRANSACTIONS ON INDUSTRIAL ELECTRONICS, IEEE TRANSACTIONS ON INDUSTRIAL INFORMATICS, IEEE TRANSACTIONS ON SERVICES COMPUTING, and IEEE TRANSACTIONS ON SOFTWARE ENGINEERING. He received the Best Paper Award in ICSOC 2016 and the Best Short Paper Award Nomination in ICSOC 2021. His research interests include services computing, distributed systems, cyber security, software testing, machine learning, and data analytics.

HAO CHEN received the bachelor's degree in computer science and technology from Yangzhou University, in 2021. He is currently pursuing the M.S. degree with the College of Computer and Information, Hohai University, Nanjing, China. His current research interests include data mining and AI testing.